

# Conversion of EBSD data by a quaternion based algorithm to be used for grain structure simulations

A. Melcher, A. Unser, M. Reichhardt, B. Nestler, M. Pötschke, M. Selzer

*Over the last decades, great progress has been made in developing models to describe and simulate the time-spatial evolution of microstructure in polycrystals. A major problem is to find suitable initial conditions to start such a simulation.*

*One possibility to solve this problem is the usage of experimental data given by Electron Back Scattering Diffraction (EBSD) measurement. These technique provides the grain structure of a polycrystal in terms of Eulerian angles.*

*In this work, we introduce a algorithm based on quaternions to describe the reconstruction of a polycrystal from the EBSD data in two and three space dimensions. We describe the EBSD measurement and the mathematical background in detail. From this we deduce the reconstruction algorithm and give some simulation results.*

## 1 Introduction

In material sciences it is important to characterize the microstructure and texture of the material under investigation. Misorientation, grain size, grain shape, grain boundary character, grain orientation and texture distribution can have significant influence on the properties of the material. To measure the microstructure and texture of a material optical microscopy, Scanning Electron Microscopy (SEM), Transmission Electron Microscopy (TEM) or neutron and X-ray diffraction can be used to obtain local information of the microstructure.

In the last years, the automated Electron Backscatter Diffraction (EBSD), also known as Orientation Imaging Microscopy (OIM), has become increasingly important for the quantitative characterization of the grains, subgrains and microtextures. This technique is applicable for materials with crystallographic character like metals, minerals, semiconductors or ceramics, also most of inorganic crystalline materials (Maitland and Sitzman, 2006).

The EBSD technique allows for the automatic and direct measurement of a large amount of orientations in terms of Eulerian angles in a cross-section of a specimen. Therefore, the EBSD technique is a priori a 2D measurement of a 3D information in a specimen.

The main advantage of the EBSD technique lies in the direct access to the local orientation of the material in a measurement point or in the relation between the microstructure and crystallography (K.Kunze et al., 1993). The popularity of EBSD in connection with SEM is due to the fact, that for the time being it gives the most reliable spatial resolution and angular precision to describe microstructures. It is also possible to process large data sets and analyze them quickly due to the increasing power of computers (Cho et al., 2005). The EBSD technique enables the user to post process the data for a subsequent analysis, like a finite element method, for considering microstructure and texture or grain growth simulation. For a complete review of the topic refer to (Rollett et al., 2007).

In the sequel we describe an algorithm, where we can reconstruct an average or mean orientation for the grains and the grain structure from the EBSD measurement based on the given lattice orientations. This algorithm can be applied to 2D and 3D measurements.

Several attempts are proposed to solve this task in the 2D case, like a nonlinear method presented by (Barton and Dawson, 2001) or a statistical analysis of the orientation data given by (Krieger Lassen et al., 1994). Our approach is based on quaternion algebra as proposed in the works of (Cho et al., 2005) and (Humbert et al., 1996), where in the last work an approach based on orthogonal matrices is introduced as well.

To identify a grain from EBSD measurement, one has to determine the grain boundary and the average orientation inside this grain. To fulfill this task, it is useful to do the necessary computations in terms of misorientation over the set of all measurement points inside the grain. There are three major types of misorientations which can be used to determine the misorientation inside a grain. First one can express the magnitude of misorientation over all measurement points inside a grain called grain orientation spread (GOS). The second one is computed between

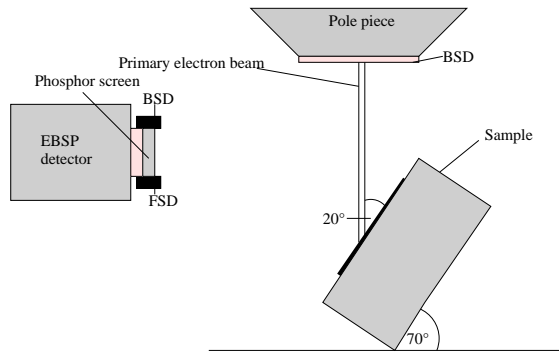


Figure 1: Scheme of an EBSD measurement unit

each measurement point and the mean orientation called scalar orientation spread (SOS). Within this work we use a third possibility called grain average misorientation (GAM), whereby the misorientation is only calculated from adjacent measurement points only, which give a nearest neighbour correlation.

The aim of this work is to give a short review of the mathematical background to describe orientation and rotation. We will give the connection between the several representations of orientation respectively rotation like quaternions, rotation matrices and others. Based on this background, we develop an algorithm to reconstruct the orientation and grain structure from EBSD data in two and three space dimensions.

This paper is organized as follows. In chapter 2 we give a short technical review of the EBSD measurement, followed by an introduction of the mathematical theories for evaluating the EBSD-measurement in chapter 3. The conversion algorithm is given in chapter 4 followed by simulation results in chapter 5 using phase-field simulations. We close this paper with a summarizing conclusion and an outlook of possible future works.

## 2 The physical setup of the EBSD technique

In the sequel, we give a short survey of the physical background and the function of the EBSD technique. First we introduce the EBSD technique in 2D and then give a short summary of the applications of EBSD measurement to 3D problems. Further detailed information can be found in (Maitland and Sitzman, 2006) and (Schwartz et al., 2009).

From the historical point of view, the development of the EBSD-technique started in 1928 with the work of Kikuchi. An electron beam of 50 keV was directed on a cleavage face of calcite at a grazing incidence of  $6^\circ$ , where diffraction patterns were recorded on photographic plates behind and in front of the crystal. The modern development of the EBSD technique started in the mid eighties of the last century with the work of (Dingley, 1984) and is still under development until the present time, for example see the works of (Khorashadizadeh et al., 2008) and (S.Zaefferer et al., 2008).

### 2.1 How does EBSD work?

An EBSD measurement can be performed in a scanning electron microscope (see Figure 1). One needs a flat highly polished sample, that is arranged under a shallow angle in general of  $10^\circ - 20^\circ$  to the incident electron beam. The technical parameters of the electron beam are typical: an accelerating voltage of 10 – 30 kV and a current between 1 – 50 nA. The working distance to the tilted sample ranges between 10 – 15 mm. The electron beam interacts with the crystal of the sample, and the diffracted electrons form a pattern (Electron Backscattering Pattern (EBSP)) on a fluorescent screen, which was between 150 – 170 mm away. This pattern is characteristic of the crystal structure and orientation of the sample region, from which it was generated. See (Wells, 1999) for more details of the electron-crystal interaction. The spatial resolution of the technique depends on the capabilities of the underlying SEM optic. In general, an EBSD measurement is the scan of all measurement points  $(x_i, y_i)$  of the sample with distances  $\Delta x$  and  $\Delta y$  between two measurement points.

The EBSP detector is a digital camera, where the CCD chip is illuminated by the phosphor screen which converts the diffracted electrons into light suitable for the CCD camera to record. This data is evaluated with commercial software provided together with the EBSD hardware. The Kikuchi bands included in the EBSP are analyzed using the Hough transform (see (J. Illingworth and J. Kittler, 1988) for a survey). With a priori information of the underlying phase of the crystal, the software is able to determine all possible orientations in every measurement point. In consequence, EBSD gives a rise to 3D information of the underlying crystal coming from the 2D EBSP

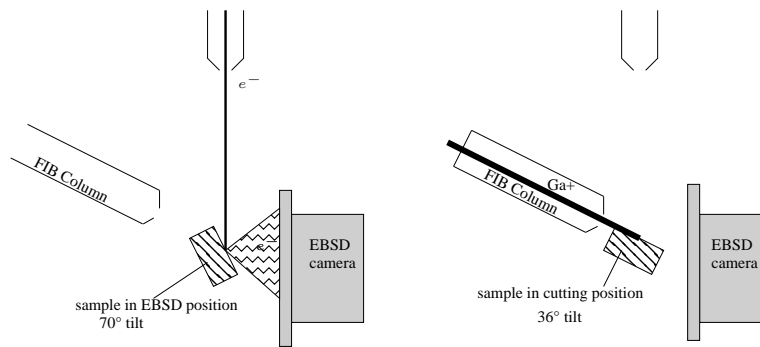


Figure 2: Scheme of a combined EBSD FIB measurement unit

on the phosphor screen in every measurement point.

## 2.2 Data measurement

The data set generated by the EBSD software for the measurement procedure is quite simple. It is a database, where a row coincides with a measurement point, and a column represents a measured parameter. During the EBSD measurement at every point of the sample, an EBSP is captured and analyzed. The software gives as a solution the identified parameters or a zero solution. Zero solutions come from measurements, where the software is unable to detect an EBSP due to several reasons, like sample surface deformations or measurement at grain boundary with overlapping EBSP. If the analysis of the software is successful, the most important information are the phases, if more than one match unit is specified by the user, and orientation in terms of Eulerian angles.

## 2.3 Three-dimensional EBSD

As outlined above, the conventional EBSD technique for characterizing microstructures of a material is restricted to the measurement of 3D information in a 2D plane cut of the sample. Statistical methods can give some additional information on the underlying 3D structure of the material, however in many cases the knowledge of the 3D characterization of the sample is of vital importance, like the true size and shape of grains for grain growth investigations.

The characterization of materials in three space-dimensions can be done in two ways. Either by applying transmissive radiation to gain the information, or the serial sectioning of a sample. In this work we restrict ourselves to the second possibility.

Serial sectioning can be done in several ways, e.g. mechanical cutting, polishing, chemical polishing, etching and others, and for all microscopy techniques are available. The main difficulty is the control of the sectioning depth and the production of flat and parallel surfaces to get good measurements. The alignment of the sample must be correct, as well, many of the sectioning techniques are labour intensive. A technique to overcome these difficulties in serial sectioning is the usage of a dual beam system consisting of an EBSD unit and a Focused Ion Beam (FIB)-Unit in a SEM. The FIB consists of accelerated  $Ga^+$ -ions and the impact of the beam on the surface of a sample leads to the sputtering of material, and can, therefore, be used to perform a cut in the length-scale of several nm. Further information can be found in (S.Zaefferer et al., 2008) and the references therein. A scheme of the dual unit can be found in Figure 2.

## 3 Mathematical background of orientation, misorientation and mean orientation

In this section, we introduce the mathematical basics of the terms orientation, mean orientation, misorientation and rotation. A detailed theory can be found in the books (Bunge, 1969) and (Morawiec, 2004).

### 3.1 Orientation and misorientation

If we work with the topic of orientation in considering crystallites or polycrystals, both the sample and the crystal symmetry have to be considered, because several equivalent orientations can exist depending on the symmetry

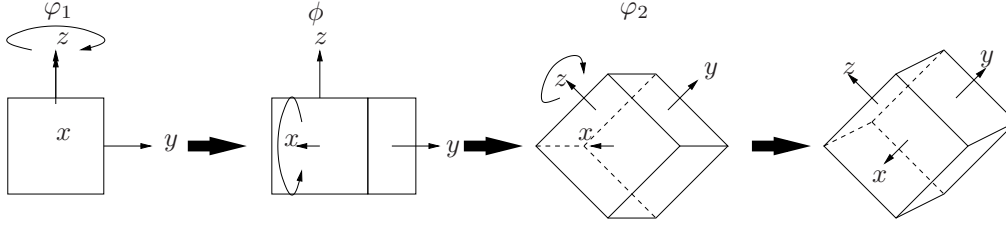


Figure 3: Eulerian angles in Bunge notation

of the sample and the symmetry of the crystal. For example, if a cubic symmetry is considered, there are 24 possibilities to arrange a crystal by using a proper rotational symmetry operator. This means that an orientation can be expressed by 24 equivalent possibilities (Humbert et al., 1995) and (Bhattacharya, 2003).

In general, an orientation can be described by three parameters combined in the symbol  $g$ . Introduced by (Bunge, 1969), the orientation space or Eulerian space (Euler 1775) consists of every orientation  $g$ , which transforms a sample coordinate  $K_S$  in a crystal coordinate  $K_C$ . In this work, we restrict ourselves to the so-called Bunge Euler angles, i.e. that an orientation can be expressed through three rotations with the angles  $(\varphi_1, \phi, \varphi_2)$ . Given a fixed coordinate system with the  $x$ -,  $y$ -,  $z$ -axes, we perform the following rotations (see Figure 3)

1. A rotation of an angle  $\varphi_1$  about the  $z$ -axis.
2. A rotation of an angle  $\phi$  about the rotated  $x$ -axis.
3. A rotation of an angle  $\varphi_2$  about the rotated  $z$ -axis.

Now, the finite dimensional space of orientation is given by

$$\begin{aligned} g &: [K_S \rightarrow K_C] \text{ or } g^{-1} = g^T : [K_C \rightarrow K_S] \\ G &: 0 \leq \varphi_1, \varphi_2 < 2\pi; 0 \leq \phi \leq \pi. \end{aligned} \quad (1)$$

In the sequel we refer to  $g = \{\varphi_1, \phi, \varphi_2\}$  as the Bunge-Euler angles notation. Rotations have in general the following properties (Bunge, 1969):

- The composition of two rotations  $g_1$  and  $g_2$  is again a rotation  $g : g = g_2 \cdot g_1$ .
- Rotation constitutes a group  $\mathcal{G}$  in the mathematical sense, i.e.  $\forall g \in \mathcal{G} \rightarrow g^{-1} \in \mathcal{G}$ , where in  $g^{-1}$  denotes the inverse rotation and is given in terms of Eulerian angles as  $g^{-1} = \{\pi - \varphi_2, \phi, \pi - \varphi_1\}$ , and the identical rotation is given as  $e = \{0, 0, 0\}$ .
- If a rotation  $g$  is known, the orientation of a crystal in a polycrystalline sample is characterized unique. But we can not characterize a rotation  $g$  in a unique form from crystal orientation. The reason lies in the crystal symmetry. A detailed discussion can be found in (Bunge, 1969).
- If we neglect the crystal symmetry and consider two orientations or rotations  $g$  and  $g'$ , then the misorientation or distance of orientations is  $\Delta g = g^{-1} \cdot g'$ .

For the parametrization of rotations or orientations there exist several possibilities. An Eulerian angle is a degree of freedom, that represents a rotation about one of the coordinate axes. An alternative representation is, that a rotation can be described via a  $3 \times 3$  orthogonal matrix. The connection between the Bunge-Euler angles and a rotation matrix is

$$\begin{aligned} \mathbf{g}(\varphi_1, \phi, \varphi_2) &= \begin{bmatrix} \cos \varphi_1 & -\sin \varphi_1 & 0 \\ \sin \varphi_1 & \cos \varphi_1 & 0 \\ 0 & 0 & 1 \end{bmatrix} \begin{bmatrix} 1 & 0 & 0 \\ 0 & \cos \phi & -\sin \phi \\ 0 & \sin \phi & \cos \phi \end{bmatrix} \begin{bmatrix} \cos \varphi_2 & -\sin \varphi_2 & 0 \\ \sin \varphi_2 & \cos \varphi_2 & 0 \\ 0 & 0 & 1 \end{bmatrix} \\ &= \begin{bmatrix} \cos \varphi_1 \cos \varphi_2 - \sin \varphi_1 \cos \phi \sin \varphi_2 & -\cos \varphi_1 \sin \varphi_2 - \sin \varphi_1 \cos \phi \cos \varphi_2 & \sin \phi \sin \varphi_1 \\ \sin \varphi_1 \cos \varphi_2 + \cos \varphi_1 \cos \phi \sin \varphi_2 & -\sin \varphi_1 \sin \varphi_2 + \cos \varphi_1 \cos \phi \cos \varphi_2 & -\sin \phi \cos \varphi_1 \\ \sin \phi \sin \varphi_2 & \sin \phi \cos \varphi_2 & \cos \phi \end{bmatrix}. \end{aligned} \quad (2)$$

More details about the properties of rotation matrices can be found for example in (Morawiec, 2004).

If we deal with orientations and rotations, another useful tool is the use of the quaternion algebra, especially the use of unit quaternions. The main advantage of this representation is, that the singularity, which appears in Euler spaces at the origin is avoided. It is easy to see, that in Euler space, the first and third angle becomes linear dependent, if the second angle is zero.

A unit quaternion is defined as a real vector in  $\mathbb{R}^4$ :

$$q = (q_0; \mathbf{q}) = (q_0; q_1, q_2, q_3) \text{ with } \sum_{i=0}^3 q_i^2 = 1. \quad (3)$$

The connection between the Eulerian angles in Bunge notation, unit quaternions is given in (Cho et al., 2005), (Rollett et al., 2007), (Humbert et al., 1996). More detailed information can be found in the book (Morawiec, 2004) and the short review (Morawiec and Pospiech, 1989):

$$q = \left[ \cos \frac{\omega}{2}, \sin \frac{\omega}{2} n_1, \sin \frac{\omega}{2} n_2, \sin \frac{\omega}{2} n_3 \right], \quad (4)$$

and

$$q = \left[ \cos \frac{\phi}{2} \cos \frac{\varphi_1 + \varphi_2}{2}, \sin \frac{\phi}{2} \cos \frac{\varphi_1 - \varphi_2}{2}, \sin \frac{\phi}{2} \sin \frac{\varphi_1 - \varphi_2}{2}, \cos \frac{\phi}{2} \sin \frac{\varphi_1 + \varphi_2}{2} \right], \quad (5)$$

where  $\omega$  denotes the rotation angle and  $\mathbf{n} = (n_1, n_2, n_3)^T$  the rotation axis. The inverse relation from the equations (4) and (5) can be found in appendix A. The quaternion corresponding to an inverse rotation  $g^{-1}$  is given as

$$q^{-1} = (q_0; -\mathbf{q}) = (q_0; -q_1, -q_2, -q_3). \quad (6)$$

If we consider the rotation  $g = g_1 \cdot g_2$ , the corresponding quaternion  $q$  is the multiplication of the two quaternions  $q_1$  and  $q_2$  associated to the rotations  $g_1$  and  $g_2$ :

$$q_1 \cdot q_2 = (q_{0,1}q_{0,2} - \mathbf{q}_1 \cdot \mathbf{q}_2; q_{0,1}\mathbf{q}_2 + q_{0,2}\mathbf{q}_1 + \mathbf{q}_1 \times \mathbf{q}_2). \quad (7)$$

The misorientation in terms of quaternions is then

$$\Delta q = \Delta q(q_1, q_2) = q_1^{-1} \cdot q_2, \quad (8)$$

respectively

$$\Delta q(q_1, q_2) = (q_{0,1}q_{0,2} + \mathbf{q}_1 \cdot \mathbf{q}_2; q_{0,1}\mathbf{q}_2 - q_{0,2}\mathbf{q}_1 - \mathbf{q}_1 \times \mathbf{q}_2), \quad (9)$$

where  $q_i$ ,  $i = 1, 2$  belongs to the rotation  $g_i$ ,  $i = 1, 2$  with  $\Delta g = g_1^{-1} \cdot g_2$ .

If we take the crystal symmetry into account, the possible misorientations are

$$M_i = \Delta q \cdot S_i, \quad i = 1, \dots, K, \quad (10)$$

where  $K$  is the amount of the crystal-symmetry dependent possibilities to express an orientation. The  $S_i$  are the possible realizations of the symmetry operation. From all this possible misorientations, we take the minimum

$$M := \min_{i=1}^K M_i, \quad (11)$$

to get a unique representation of misorientation.

Since the misorientation is given in terms of a quaternion, the corresponding misorientation angle  $\Phi$  can easily be computed from the corresponding Rodriguez vector (Morawiec and Field, 1996):,

$$\mathbf{R}(\Phi, \mathbf{n}) = \frac{1}{q_0} (q_1, q_2, q_3) = \tan \frac{\Phi}{2} \mathbf{n} \text{ with } |\mathbf{n}| = 1, \quad (12)$$

where  $\Phi$  describes the rotation angles and  $\mathbf{n}$  the rotation axis.

We remark that the equations (4) and (5) state a two to one homomorphism between the group of unit quaternions and the group  $\mathcal{SO}(3)$ , i.e. the quaternions  $q_1 = \left[ \cos \frac{\Phi}{2}, \sin \frac{\Phi}{2} \mathbf{n} \right]$  and  $q_2 = \left[ \cos \frac{\Phi + 2\pi}{2}, \sin \frac{\Phi + 2\pi}{2} \mathbf{n} \right]$  represent the same rotation  $\mathbf{R}(\Phi, \mathbf{n})$ . A unit quaternion can be considered as a point of the surface on the four-dimensional unit sphere  $\mathbb{S}^3$ . The definition of the Rodrigues vector can be considered as the geodesic projection from  $\mathbb{S}^3$  to  $\mathbb{R}^3$ . In the sequel, we take advantage of the representation of rotations in terms of quaternions for computing the misorientations and the mean orientations. For the representation and visualization of the orientation distribution it is better to use the Rodrigues vector due to the fact, that it exhibits a one to one relation between orientation and their presentation. Some useful additional formulas concerning this topic can be found in appendix A.

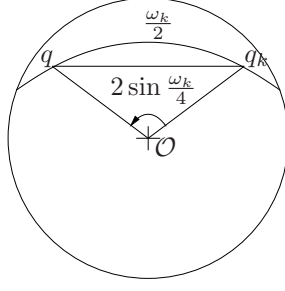


Figure 4: Geodesic and Euclidean distance of the unit sphere  $\mathbb{S}^3$

### 3.2 Average of orientations

In this section we give a short review on how the average orientation can be computed from a set of orientations. According to (Humbert et al., 1996), the average of orientations can be computed using quaternions or rotation matrices. Using unit quaternions, we have first to introduce a suitable distance on the surface of the four-dimensional unit sphere  $\mathbb{S}^3$  (see Figure 4). Two possibilities are the geodesic distance, which is the angular distance, or the Euclidean distance.

The Euclidean distance is

$$d_k^2 = \|q - q_k\|^2 = \|I - q_k q^{-1}\|^2 = 4 \sin^2 \frac{\omega_k}{4}. \quad (13)$$

When using the well known trigonometric relation  $\sin^2 \frac{x}{2} = \frac{1}{2} (1 - \cos x)$  with  $x = \frac{\omega_k}{2}$  yields

$$d_k^2 = 4 \sin^2 \frac{\omega_k}{4} = 2 \left(1 - \cos \frac{\omega_k}{2}\right) = 2(1 - (q_0 q_{k,0} + \mathbf{q} \cdot \mathbf{q}_k)), \quad (14)$$

using the fact, that  $\cos \frac{\omega_k}{2}$  is the first component of the quaternion  $q \cdot q_k$ .

The center of mass of rotations  $g$  represented by the quaternion  $q$  can now be determined by minimizing the metric distance. For a given set  $g_k$ ,  $k = 1, \dots, N$  of orientations let  $q_k$  be the corresponding quaternions. We now introduce the objective function  $f(q, q_1, \dots, q_k)$  from equation (14) as

$$f(q, q_1, \dots, q_k) = \frac{1}{N} \sum_{k=1}^N 2[1 - (q_0 q_{k,0} + \mathbf{q} \cdot \mathbf{q}_k)]. \quad (15)$$

Remember, that the quaternion  $q$  is a unit quaternion, therefore, we have the constraint  $\|q\|^2 = q_0 q_0 + \mathbf{q} \cdot \mathbf{q} = 1$  in our minimization problem. Which yields with a Lagrange multiplier and the introduction of the modified objective function  $\hat{f}(q, q_1, \dots, q_k, \lambda)$

$$\hat{f}(q, q_1, \dots, q_k, \lambda) = f(q, q_1, \dots, q_k) + \lambda(\|q\|^2 - 1). \quad (16)$$

To determine the minima, we have to solve

$$\frac{\partial \hat{f}(q, q_1, \dots, q_k, \lambda)}{\partial q_i} = \frac{\partial}{\partial q_i} \left\{ \frac{1}{N} \sum_{k=1}^N 2(1 - (q_0 q_{k,0} + \mathbf{q} \cdot \mathbf{q}_k)) + \lambda(q_0 q_0 + \mathbf{q} \cdot \mathbf{q} - 1) \right\} = 0, \quad (17)$$

for  $i = 0, 1, 2, 3$ . These condition gives

$$q_i = \frac{1}{N} \sum_{k=1}^N q_{i,k} \cdot \frac{1}{\lambda}, \quad i = 0, 1, 2, 3, \quad (18)$$

where  $\lambda = \frac{1}{N} \left\| \sum_{k=1}^N q_{i,k} \right\|$  due to the constraint, that  $q$  must be a unit quaternion. The last equation expresses, that the mass center of a set of unit quaternions is simple the arithmetic average of the quaternions, i.e.

$$\bar{q} = \frac{\sum_{k=1}^N q_k}{\left\| \sum_{k=1}^N q_k \right\|}. \quad (19)$$

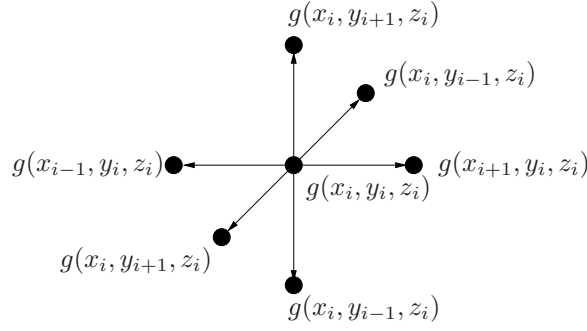


Figure 5: Adjacent orientation points in a three-dimensional grid

## 4 Reconstruction algorithm

### 4.1 Some general assumptions

Before describing the reconstruction algorithm in detail, we repeat some general ideas. We describe this ideas in such a way, that they are suitable for two- and three-dimensional EBSD-measurement.

The task is to construct a set or cloud of orientation, which has a minimum misorientation between adjacent elements. To achieve this aim, a position criterion and a criterion for the misorientation is used.

First of all we assume, that within a grain the orientations respectively orientation distribution are described via a continuous function, and there are orientation gradients inside the grain, i.e.

$$g(\mathbf{x}) = \{g(\mathbf{x}) \mid \forall \mathbf{x} \in \text{a grain } j\}$$

$$\text{with } \lim_{\Delta \mathbf{x} \rightarrow 0} \frac{m(\mathbf{x}, \mathbf{x} + \Delta \mathbf{x})}{\Delta \mathbf{x}} = 0, \quad (20)$$

where  $m(\mathbf{x}, \mathbf{y}) \in \mathbb{R}^n \times \mathbb{R}^n \mapsto \mathbb{R}$  denotes the misorientation function,  $g(\mathbf{x})$  the orientation function depending on their representation and  $\mathbf{x} \in \mathbb{R}^n$ ,  $n = 2, 3$  the position.

If we consider the data coming from an EBSD measurement, the orientations at the measurement points have only a discrete distribution depending on the grid size, i.e.

$$g(\mathbf{x}_i) = \{g(\mathbf{x}_i) \mid \forall \mathbf{x}_i \in \text{a grain } j\}$$

$$\text{with } \lim_{\Delta \mathbf{x} \rightarrow \delta} \frac{m(\mathbf{x}, \mathbf{x} + \Delta \mathbf{x})}{\Delta \mathbf{x}} = \theta, \quad (21)$$

where  $\delta$  is the spatial stepsize of the measurement and  $\theta$  the misorientation angles allowed inside a grain. As consequence, if the discrete orientation function  $g(\mathbf{x}_i)$  is given, we can deduce, that the misorientation between the adjacent points is smaller than for the points that are more remote. In general, there are four respectively six adjacent points in a rectangular grid and, therefore, the search for adjacent points is made for all four/six direction (see Figure 5). We note, that these amount can be reduced to two/three points, if we take the fact into account that the rotation angle between two rotations  $g_1$  and  $g_2$  is equal to the rotation angle between  $g_2$  and  $g_1$ . Only the rotation axis have opposite signs.

In our algorithm, the following position criterion for the misorientations must be satisfied

$$\theta(\mathbf{x}_i, \mathbf{x}_j) \leq \theta^{crit}$$

$$\theta(\mathbf{x}_i, \mathbf{x}_j) = m(g(\mathbf{x}_i), g(\mathbf{x}_j)), \quad (22)$$

where  $\mathbf{x}_i$  and  $\mathbf{x}_j$  are adjacent measurement points and  $\theta^{crit}$  is the critical misorientation angle. In addition, we also have to take the crystal symmetry into account. If the crystal symmetry provides  $M$  equivalents for an orientation, we have to consider  $M$  sets of orientations for the measurement points of a grain. Only these orientations are included in every set with the smallest misorientation between the adjacent points. In terms of quaternions we have to compute

$$q^k(\mathbf{x}) = q(\mathbf{x}) \cdot S_k, \quad k = 1, \dots, M$$

$$q^{res}(\mathbf{x}) = q^k(\mathbf{x}) \text{ if } \min\{\Delta q(q^j(\mathbf{x}), q^k(\mathbf{x}))\}, \quad (23)$$

where  $q^j(\mathbf{x})$ ,  $j = 1, \dots, 6$  denotes an adjacent quaternion to the quaternion  $q(\mathbf{x})$ ,  $S_k$  the crystal symmetry operator. Then the average orientation is given as

$$\bar{q} = \frac{\tilde{q}}{\|\tilde{q}\|} \text{ with } \tilde{q} = \frac{1}{V_{grain}} \int_{V_{grain}} q^{res}(\mathbf{x}) d\mathbf{x} \quad (24)$$

or

$$\bar{q} = \frac{\tilde{q}}{\|\tilde{q}\|} \text{ with } \tilde{q} = \frac{1}{N} \sum_{l=1}^N q_l^{res}(\mathbf{x}), \quad (25)$$

where  $q_l^{res}(\mathbf{x})$  is a representative quaternion corresponding to an orientation  $g(\mathbf{x})$ , and  $V_{grain}$  the area or volume of the concerned grain.

## 4.2 Stepwise description of the reconstruction algorithm

In the following section we describe the conversion algorithm for EBSD data into simulation data, which uses the previously introduced techniques. The algorithm consists of the following steps:

- i) **Read EBSD measured Euler angles:** In general, raw EBSD data are provided as a list of measurement points. Typically such a list contains the coordinates and measured Euler angles. To determine the size of the domain we scan all measurement points. After this step we gain a domain filled with continuous Euler angles, see Fig. 6 a).
- ii) **Correction of measurement gaps:** Often there are measurement gaps containing no data, marked by an Euler angle (0.0, 0.0, 0.0). To allow a proper reconstruction it is necessary to remove as many as possible of these gaps. One obvious way is to copy a value from a neighbouring point. Another possibility is to average neighbouring points to get a value, but this often results in an even worse point when averaging between two adjacent grains. Figure 6 b) shows the data after removing of the measurement gaps by copying the *left* neighbour angle.
- iii) **Clustering using neighbour misorientations:** In the next processing step the continuous angles are grouped to form a continuous grain. The basic idea is to start a flooding algorithm to cluster all measurement points which are similar to their neighbours.

We start at a point named  $s_0$  which is not assigned to any grain. This point is marked with a unique number, the new index of the grain, further referred to as grain  $g$ . To determine if any adjacent points  $s$  are part of the current grain  $g$  we remember them in a set denoted by  $\mathcal{S}$ .

As long as  $\mathcal{S}$  is not empty there remain measurement points to be tested. We choose a point  $s \in \mathcal{S}$  and add all its neighbours already associated with grain  $g$  to a set  $\mathcal{N}$ . The set  $\mathcal{N}$  contains at least one point which is the one that added  $s$  to  $\mathcal{S}$  in the first place. If  $\theta(s, n) < \theta^{crit}$  for any  $n \in \mathcal{N}$  (see eqn. 22) we remove  $s$  from the set  $\mathcal{S}$ , add it to grain  $g$  and include all neighbors of  $s$ , not already belonging to a distinguished grain, to  $\mathcal{S}$ . By this procedure every point is assigned to a single grain, satisfying the desired  $\theta^{crit}$  which can be seen in Fig. 6 c).

- iv) **Correction of measurement errors:** We observe another main reason for fluctuations in the data. Measurement errors due to the physical limitations appear. Using such points as correct input data will result in grains expanding only over one grid cell. Another reason to reduce grains can be justified by the assumption that small grains will disappear very fast in a grain coarsening process but require (memory intensive) parametrization.

To achieve a more homogeneous structure we identify grains only composed of measurement points less than a specified threshold  $t$ . The selected grains are then mapped to an artificial grain  $g'$  which consists of points that may not be connected. Figure 6 d) shows the grain reduction result for a threshold  $t = 5$ , in which the grain  $g'$  is marked in black. In this way the number of grains was reduced from initially 759 to 339 after this step of the algorithm. Using this as an initial geometry we conducted a preconditioning simulation forcing the artificial grain to disappear.

- v) **Compute mean orientation of each grain:** Finally for each grain the measured orientations are used to compute an average orientation, as the global grain orientation, using equation (19).

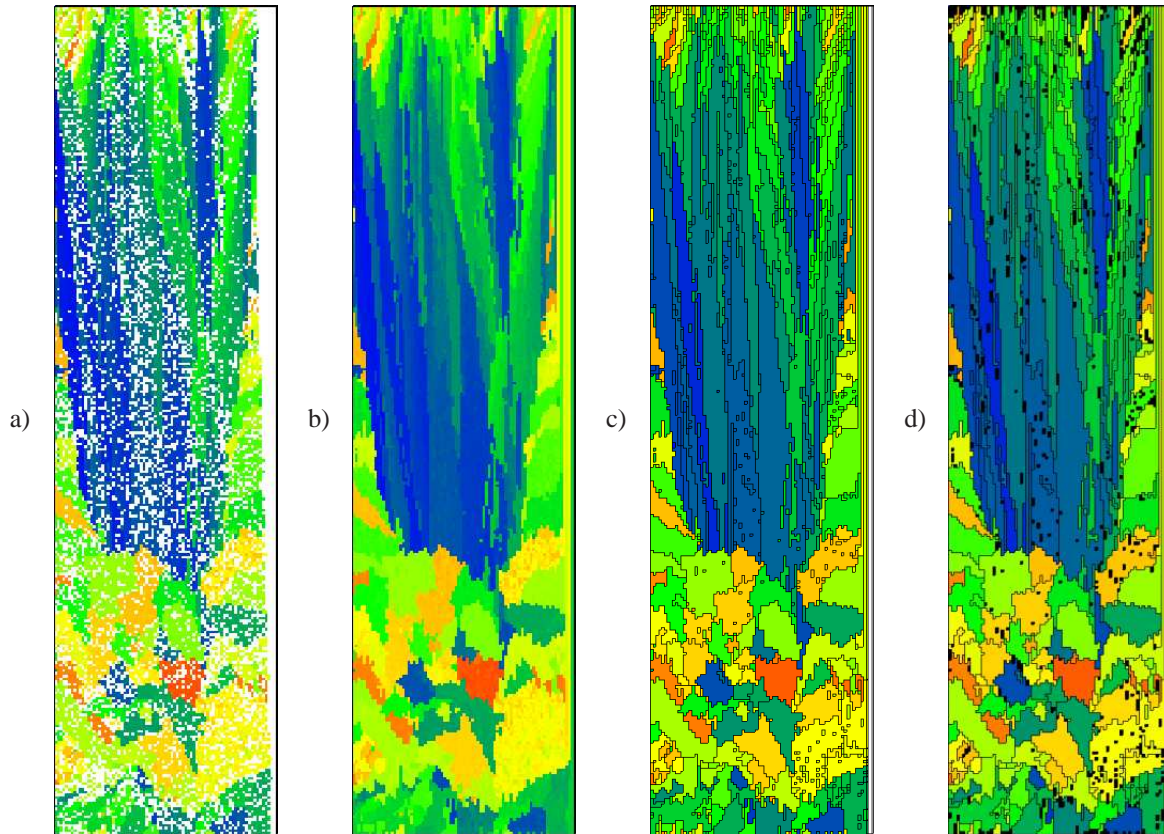


Figure 6: Data conversion processing steps: a) Raw EBSD data, b) image after removing measurement gaps, c) image after the clustering process and d) after mapping *small* grains to an artificial grain. Experimental data provided by Dr. Stefan Roth, IFW Dresden.

### 4.3 Some remarks about the reconstruction algorithm

After describing the reconstruction algorithm and the main formulas for computing the misorientation in terms of quaternions, we remark, that alternative formulations for rotation matrices (Humbert et al., 1996) and mixed formulations (K.Kunze et al., 1993) exist. The main advantage of using quaternions in comparison to rotation matrices is, that for the calculation of the misorientation in the main computation step only two quaternion multiplications are necessary in comparison to two matrix multiplications. A four dimensional quaternion multiplication needs 16 scalar multiplications and 12 scalar additions in contrast to a  $3 \times 3$  matrix multiplication for which 27 scalar multiplications and 18 scalar additions must be performed (Andrew.J.Hanson, 2006). In summary a quaternion multiplication needs only 28 simple arithmetic operations where a multiplication of two rotations matrices needs 45 simple arithmetic operations. A comparison of the reconstruction algorithm using quaternions and rotation matrices is done by the authors. The reconstruction algorithm using quaternions is 60-times faster in comparison to the usage of rotation matrices. Therefore, the speed up in large EBSD data sets should be obvious. In general, the quality of the reconstruction depends on the quality of the EBSD measurement. The reconstruction algorithm is programmed in such a way that it works for data files with measurement errors greater than 50% of the total amount of measurement points. You can get such EBSD measurements if you have plastic deformation inside the grains due to e.g. a rolling process. But the results from such data files are questionable. Another marker for the quality is the threshold of misorientation. Possible limitations of the reconstruction algorithm depend strongly on the underlying hardware e.g. the cpu speed which give a direct influence to the computation time of the algorithm, or the available memory, which gives a limitation of the maximal amount of measurement points. This limitations can be improved in using a parallelized version of the reconstruction algorithm.

## 5 Simulation Results

In the previous sections, we introduced methods of transferring and postprocessing discrete EBSD measurements in order to prepare complete and homogenized data sets for setting up large scale simulations of polycrystalline

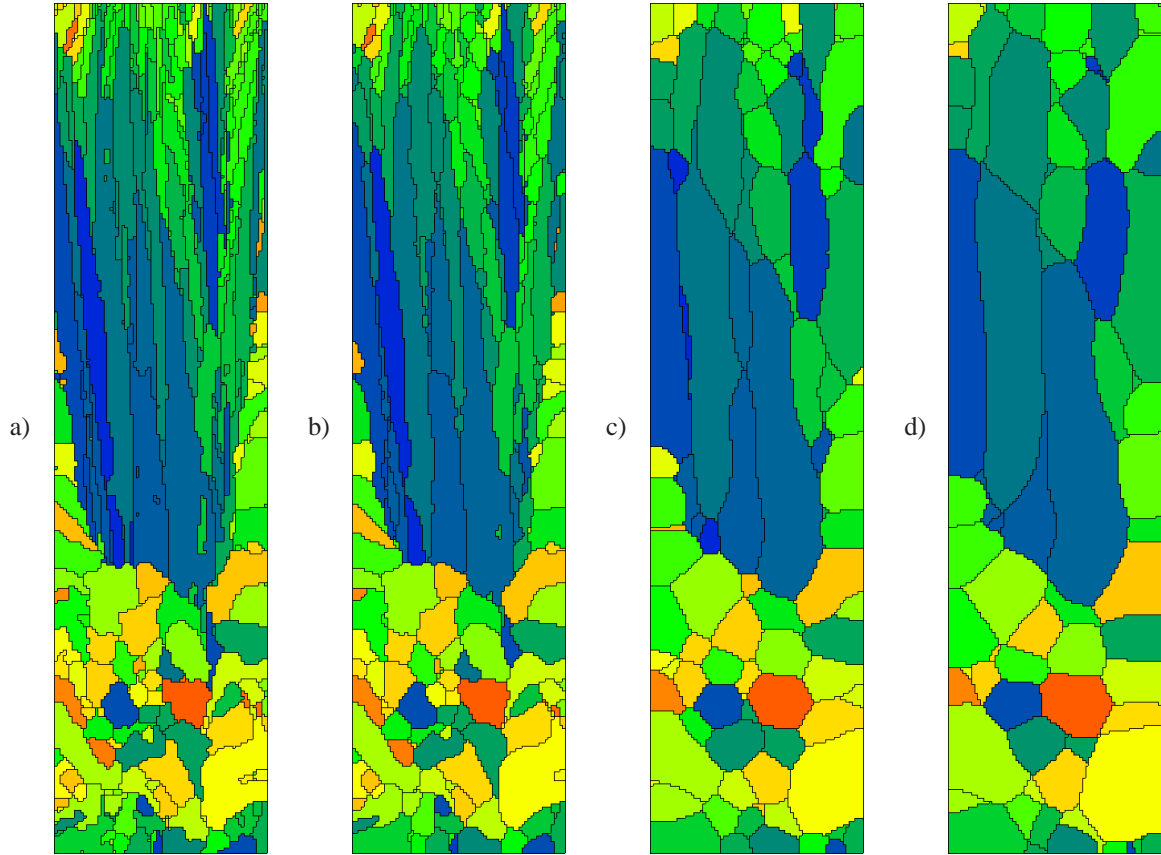


Figure 7: Time evolution of an EBSD grain structure after conversion of the data. The sample performs the characteristic features of grain growth. The different colours indicate the individual grains in a polycrystalline material.

microstructures. The reconstruction algorithm provides information of the orientation and misorientation distributions in grain structures without gaps and errors from experimental measurements. These data can be used to divide the initial computational domain in defined sections of grains with particular crystallographic orientation and allow to simulate grain structure evolution on the basis of real experimental data. Furthermore, the misorientation data sets give valuable input parameters of the grain boundary characteristics. The conversion methods find general application to any kind of microstructure simulation. To illustrate the use, we will exemplarily show phase-field simulations of coarsening processes in polycrystalline austenitic material. For that, we briefly summarize the main settings of the simulation. For a detailed understanding of the phase-field method, we refer to appropriate citations. To describe the evolution of a polycrystalline microstructure of  $N$  different grains with a phase-field model, a vector-valued order parameter  $\phi = (\phi_1, \dots, \phi_N)$  is introduced where each component  $\phi_\alpha, \alpha = 1, \dots, N$  is a non-conserved field variable depending on time and space and representing the state of each grain. The dynamics of the structure is described by a set of nonlinear partial differential equations of parabolic type for each component of  $\phi$ . The set of equations contains physical quantities of the grain boundaries, namely pairwise grain boundary mobilities and energies including crystal anisotropy and a functional dependence on the misorientation. Details of the mathematical expressions can be recalled in Nestler et al. (2005). We use the converted EBSD data for both, to fill the computational domain with an experimentally observed grain structure and to define a realistic matrix of grain boundary misorientations.

Fig. 7 shows an image sequence of a phase-field simulation of a grain growth process in temporal order as can be seen in heat treatment applications of manufacturing processes. The dynamic behaviour is the result of a minimization of the total free energy in the system by reduction of mean curvature. The growth of the mean grain size is a characteristic behavior of grain coarsening in polycrystalline structures and can be derived from an empiric exponential power law for the mean grain diameter in time. Following (Gottstein, 2007), the evolution of the mean grain diameter  $d_t$  at time  $t$  is described by

$$d_t^m - d_0^m = kt, \quad (26)$$

where  $d_0$  is the initial mean grain diameter,  $m$  the grain growth exponent and  $k$  is the gradient energy coefficient.

In our simulations we used  $k = 1.0$ . If we assume that  $d_0 \ll d_t$  the equation can be simplified to

$$d_t \cong \bar{k}t^m. \quad (27)$$

For isotropic grain growth, the exponent is typically  $m = 2$ . In the phase-field simulation based on the converted EBSD data, we measured a higher exponent of  $m = 2.39$ . The accelerated growth can be explained by the strong inhomogeneity of the initial grain size distribution and by the anisotropy of the grain boundaries.

## 6 Conclusion and outlook

The presented methods of reconstructing EBSD data for the use by microstructure simulations contribute to the aim of establishing simulation environments that allow for a most realistic computational study of structure formation processes. A successive algorithm has been presented showing results of a stepwise conditioning of experimentally measured data. Because of the general form of the algorithm, the methods are applicable to almost all simulation techniques working on the length scale of grain structures.

An investigation of grain structure evolution in differently prepared samples of magnetic shape memory alloys in comparison with experimental results is in preparation. Furthermore, an extensive simulation study of large-scale 3D grain systems on the basis of EBSD data sets will be generated in a forthcoming paper.

## A Appendix

In this section we give some useful additional formulas for the relation between rotation matrix and quaternion. A rotation matrix  $\mathbf{g}$  is given in general as

$$\mathbf{g} = \begin{bmatrix} g_{11} & g_{12} & g_{13} \\ g_{21} & g_{22} & g_{23} \\ g_{31} & g_{32} & g_{33} \end{bmatrix}, \quad (28)$$

where the elements  $g_{ij}$  are defined as the directions cosines between the axes of the crystal coordinate system  $K_C$  and the sample coordinate system  $K_S$  (Spieß, 2009). The connection between a rotation matrix and the Eulerian angles in Bunge notation is given in section 3, equation (2).

In terms of quaternions, the elements of a rotation matrix are (Morawiec and Pospiech, 1989)

$$g_{ij}(q) = (q_0^2 - q_k^2)\delta_{ij} + 2q_iq_j + 2\epsilon_{ijk}q_0q_k, \quad (29)$$

where we have used the summation convention in the first term of the last equation. This gives (Cho et al., 2005)

$$\mathbf{g}(q) = \begin{bmatrix} q_0^2 + q_1^2 - q_2^2 - q_3^2 & 2(q_1q_2 - q_0q_3) & 2(q_1q_3 + q_0q_2) \\ 2(q_1q_2 + q_0q_3) & q_0^2 - q_1^2 + q_2^2 - q_3^2 & 2(q_2q_3 - q_0q_1) \\ 2(q_1q_3 - q_0q_2) & 2(q_2q_3 + q_0q_1) & q_0^2 - q_1^2 - q_2^2 + q_3^2 \end{bmatrix}. \quad (30)$$

The Inversion of the last equation is (Cho et al., 2005)

$$\begin{aligned} q_0 &= \frac{\sqrt{g_{ii} + 1}}{2}, \\ q_i &= \frac{\epsilon_{ijk}g_{jk}}{4q_0} = \frac{\epsilon_{ijk}g_{jk}}{2\sqrt{g_{ii} + 1}}, \text{ if } q_0 \neq 0, \end{aligned} \quad (31)$$

where  $\epsilon_{ijk} = \begin{cases} 1 & \text{if } (ijk) \text{ is an even permutation of } (123) \\ -1 & \text{if } (ijk) \text{ is an odd permutation of } (123) \\ 0 & \text{else} \end{cases}$

If  $q_0 = 0$  one has to solve the system

$$-q_k^2\delta_{ij} + 2q_iq_j = g_{ij}, \quad (32)$$

where  $q_k^2 \equiv 1$ . Again, we have used the summation convention.

In section 3, equation (4), we have expressed a unit quaternion in terms of rotation angle and rotation axis. From this formula we can also express the rotation angle and axis in terms of a unit quaternion as (Cho et al., 2005)

$$\cos \Phi = 2q_0^2 - 1,$$

$$\sin \Phi = 2q_0\sqrt{1 - q_0^2}, \quad (33)$$

and if  $\Phi \neq 0$

$$n_i = \frac{q_i}{\sqrt{1 - q_0^2}}. \quad (34)$$

Finally, we give the reverse relation between a unit quaternion and the Eulerian angles in Bunge notation:

$$\cos \phi = (q_0^2 + q_3^2) - (q_1^2 + q_2^2), \quad (35)$$

$$\sin \phi = 2\chi, \quad (36)$$

$$\cos \varphi_1 = \frac{q_0q_1 - q_2q_3}{2\chi}, \quad (37)$$

$$\sin \varphi_1 = \frac{q_0q_2 + q_1q_3}{2\chi}, \quad (38)$$

$$\cos \varphi_2 = \frac{q_0q_1 + q_2q_3}{2\chi}, \quad (39)$$

$$\sin \varphi_2 = \frac{q_1q_3 - q_0q_2}{2\chi}, \quad (40)$$

where  $\chi = \sqrt{(q_0^2 + q_3^2)(q_1^2 + q_2^2)} \neq 0$ . In the case where  $\chi = 0$  we have to distinguish two cases:

- $q_1 = q_2 = 0$  gives  $\phi = 0$  and  $\cos \varphi_1 + \varphi_2 = q_0^2 - q_3^2$ ,  $\sin \varphi_1 + \varphi_2 = 2q_0q_3$ .
- $q_0 = q_3 = 0$  gives  $\phi = \pi$  and  $\cos \varphi_1 - \varphi_2 = q_1^2 - q_2^2$ ,  $\sin \varphi_1 - \varphi_2 = 2q_1q_2$ .

**Acknowledgment** This work is partially supported by the German Reserach Foundation DFG under the grant SPP 1239. The authors are thankful to Dr. Andrea Böhm (Fraunhofer IWU Dresden) and Dr. Stefan Roth (IFW Dresden) for providing the EBSD data sets and their support.

## References

- Andrew.J.Hanson: *Visualizing Quaternions*. Morgan Kaufmann Publishers (2006).
- Barton, N.; Dawson, P.: A methodology for determining average lattice orientation and its application to the characterization of grain substructure. *Metallurgical And Materials Transactions A*, 32A, (2001), 1967–1975.
- Bhattacharya, K.: *Microstructure Of Martensite*. Oxford University Press (2003).
- Bunge, H.-J.: *Mathematische Methoden der Texturanalyse*. Akademie-Verlag Berlin (1969).
- Cho, J.-H.; Rollett, A.; Oh, K.: Determiation of a mean orientation in electron backscatter diffraction measurements. *Metallurgical And Materials Transactions A*, 36A, (2005), 3427–3428.
- Dingley, D.: On-line determination of crystal orientation and texture determination in an sem. *Proc. Royal Mic. Society*, 19, (1984), 74.
- Gottstein, G.: *Physikalische Grundlagen der Materialkunde*. Springer (2007).
- Humbert, M.; Gey, N.; Muller, J.; Esling, C.: Determination of a Mean Orientation from a Cloud of Orientations. Application to Electron Back-Scattering Pattern Measurements. *Journal of Applied Crystallography*, 29, 6, (1996), 662–666.
- Humbert, M.; Wagner, F.; Moustahfid, H.; Esling, C.: Determiation of the orientation of a parent  $\beta$  grain from the orientation of the inherited  $\alpha$  plates in the phase transformation from body-centered cubic to hexagonal close packed. *J. Appl. Cryst.*, 28, (1995), 571–576.
- J.Illingworth; J.Kittler: A survey of the hough transform. *Computer Vision, Graphics, and Image Processing*, 44, 1, (1988), 87–116.
- Khorashadizadeh, A.; Winning, M.; Raabe, D.: 3d tomographic ebsd measurements of havily deformed ultra fine grained cu-0.17wt%zr obtained from ecap. *Material Science Forum*, 584-586, (2008), 434–439.

- K.Kunze; Wright, S.; Adams, B.; Dingley, D.: Advances in automatic ebsp single orientation measurements. *Textures and Microstructures*, 20, (1993), 41–54.
- Krieger Lassen, N. C.; Juul Jensen, D.; Conradsen, K.: On the statistical analysis of orientation data. *Acta Crystallographica Section A*, 50, 6, (1994), 741–748.
- Maitland, T.; Sitzman, S.: *Scanning Microscopy for Nanotechnology*, chap. 2: Electron Backscatter Diffraction (EBSD) Technique and Material Characterization Examples, pages 41–75. Springer Science (2006).
- Morawiec, A.: *Orientations and Rotations*. Springer (2004).
- Morawiec, A.; Field, D.: Rodrigues parametrization for orientation and misorientation distributions. *Philosophical Magazine*, 73, (1996), 1113.
- Morawiec, A.; Pospiech, J.: Some information on quaternions useful in texture calculations. *Textures and Microstructures*, 10, (1989), 211–216.
- Nestler, B.; Garcke, H.; Stinner, B.: Multicomponent alloy solidification: Phase-field modelling and simulations. *Phys. Rev. E*, 71, (2005), 041609–1–041609–6.
- Rollett, A.; Lee, S.; Campman, R.; Rohrer, G.: Three dimensional characterization of microstructure by electron back-scatter diffraction. *Annual Review of Material Research*, 37, (2007), 627–658.
- Schwartz, A. J.; Kumar, M.; ( Brent L. Adams, eds.: *Electron Backscatter Diffraction in Materials Science*. Springer, 2nd ed. edn. (2009).
- Spieß, L., ed.: *Moderne Röntgenbeugung : Röntgendiffraktometrie für Materialwissenschaftler, Physiker und Chemiker*. Studium, Vieweg + Teubner, Wiesbaden, 2., überarb. und erw. Aufl. edn. (2009).
- S.Zaefferer; S.I.Wright; D.Raabe: Three-dimensional orientation microscopy in a focused ion beam-scanning electron microscope: A new dimension of microstructure characterization. *Metallurgical And Materials Transactions A*, 39A, (2008), 374–389.
- Wells, O. C.: Comparison of different models for the generation of electron backscattering patterns in the scanning electron microscope. *Scanning*, 21, 6, (1999), 368–371.

---

*Addresses:*

Dr. Andreas Melcher, Institut für Technische Mechanik, Karlsruher Institut für Technologie (KIT),  
Kaiserstraße 10, 76131 Karlsruhe. email: melcher@itm.uni-karlsruhe.de,  
Prof. Dr. Britta Nestler, Andreas Unser, Mathias Reichardt, Michael Selzer,  
Institute of Material and Processes, Hochschule Karlsruhe, Technik und Wirtschaft, Moltkestraße 30,  
76133 Karlsruhe. email: britta.nestler@hs-karlsruhe.de, unan0012@hs-karlsruhe.de,  
rema0052@hs-karlsruhe.de, michael.selzer@hs-karlsruhe.de,  
Martin Pötschke, Leibniz-Institut für Festkörper- und Werkstoffforschung Dresden, Helmholtzstraße 20 01069  
Dresden. email: m.poetschke@ifw-dresden.de